Applied Physics Letters

RESEARCH ARTICLE | JULY 27 2021

Generation and detection of 50 GHz surface acoustic waves by extreme ultraviolet pulses

A. A. Maznev ; R. Mincigrucci ; F. Bencivenga ; V. Unikandanunni; F. Capotondi ; G. Chen ; Z. Ding; R. A. Duncan ; L. Foglia ; M. G. Izzo; C. Masciovecchio ; A. Martinelli ; G. Monaco ; E. Pedersoli ; S. Bonetti ; K. A. Nelson

Appl. Phys. Lett. 119, 044102 (2021)
https://doi.org/10.1063/5.0060575
CHORUS

Applied Physics Letters ARTICLE scitation.org/journal/apl

Generation and detection of 50 GHz surface acoustic waves by extreme ultraviolet pulses

Cite as: Appl. Phys. Lett. **119**, 044102 (2021); doi: 10.1063/5.0060575
Submitted: 20 June 2021 · Accepted: 9 July 2021 ·
Published Online: 27 July 2021

A. A. Maznev,[1,a] R. Mincigrucci,[2] F. Bencivenga,[2] V. Unikandanunni,[3] F. Capotondi,[2] G. Chen,[4] Z. Ding,[4] R. A. Duncan,[1] L. Foglia,[2] M. G. Izzo,[5,6] C. Masciovecchio,[2] A. Martinelli,[7] G. Monaco,[7] E. Pedersoli,[2] S. Bonetti,[3,8] and K. A. Nelson[1]

AFFILIATIONS

[1]Department of Chemistry, Massachusetts Institute of Technology, Cambridge, Massachusetts 02139, USA
[2]Elettra-Sincrotrone Trieste, Basovizza, Italy
[3]Department of Physics, Stockholm University, Stockholm, Sweden
[4]Department of Mechanical Engineering, Massachusetts Institute of Technology, Cambridge, Massachusetts 02139, USA
[5]Department of Computer, Control, and Management Engineering, La Sapienza University, Rome, Italy
[6]Scuola Internazionale Superiore di Studi Avanzati (SISSA), Trieste, Italy
[7]Physics and Astronomy Department, University of Padova, Padova, Italy
[8]Department of Molecular Sciences and Nanosystems, Ca' Foscari University of Venice, Venice, Italy

[a)]**Author to whom correspondence should be addressed:** alexei.maznev@gmail.com

ABSTRACT

We use femtosecond extreme ultraviolet pulses derived from a free electron laser to excite and probe surface acoustic waves (SAWs) on the (001) surface of single crystal $SrTiO_3$. SAWs are generated by a pair of 39.9 nm pulses crossed at the sample with the crossing angle defining the SAW wavelength at 84 nm. Detection of SAWs is performed via diffraction of a time-delayed 13.3 nm probe pulse by SAW-induced surface ripples. Despite the low reflectivity of the sample in the extreme ultraviolet range, the reflection mode detection is found to be efficient because of an increase in the diffraction efficiency for shorter wavelengths. We describe a methodology for extracting the SAW attenuation in the presence of a thermal grating, which is based on measuring the decay of oscillations at twice the SAW frequency. The proposed approach can be used to study ultrahigh frequency SAWs in a broad range of materials and will bridge the wave vector gap in surface phonon spectroscopy between Brillouin scattering and He atom scattering.

Laser generation of surface acoustic waves (SAWs) first demonstrated by Lee and White in 1968[1] has developed into a tool widely used in acoustics and materials science. Typically, the optical generation of SAWs is combined with optical detection to yield a versatile non-contact technique that has been extensively used both for fundamental studies of wave propagation phenomena[2–4] and for applications such as materials characterization, thin film metrology, and nondestructive testing.[5–7] With femtosecond laser sources, there is virtually no upper limit on the frequency of acoustic waves that can be generated or detected optically. However, there is an upper limit on the SAW wavevector; namely, SAWs with a wavelength smaller than half the optical wavelength can be neither generated nor detected.[8] This limitation can be circumvented by using subwavelength structures such as nanoscale arrays of metal lines[9–12] but that takes away a major advantage of the laser-based approach, i.e., the ability to generate and detect frequency-tunable SAWs in a non-contact and noninvasive manner without fabricating any transducer structures.

With the recent progress in free electron lasers (FELs) and high harmonic generation,[13] femtosecond sources operating in the extreme ultraviolet (EUV) and x-ray ranges have become available. The use of EUV pulses for probing SAWs excited optically with the help of metal nanostructures was demonstrated in experiments with a high harmonic generation source.[10,11] More recently,[14] 13 nm radiation of the FERMI FEL at Trieste[15] was used to excite bulk and surface acoustic waves using the transient grating (TG) technique,[5,16,17] in which two crossed laser pulses are used for excitation and a time-delayed probe

pulse is used for detection of the excited acoustic waves. In the experiment,[14] the probe pulse was still at an optical wavelength of 400 nm, and the acoustic wavelength was 280 nm: SAWs with much shorter wavelengths could be generated by the EUV excitation but could not be detected by the optical probe. Subsequently, the TG setup at the TIMER beamline at FERMI has enabled EUV pump/EUV probe experiments,[18] in which bulk longitudinal waves and Lamb modes of thin membranes with wavelengths in the tens of nanometers range have been generated.[18,19] However, experiments[18,19] were conducted in the transmission geometry (i.e., the diffraction of the transmitted probe beam was measured). Since all materials are strongly absorbing in the EUV range, this requires samples in the form of ultrathin free-standing membranes, which severely limits the range of materials that can be investigated.

In this report, we describe reflection-mode EUV pump/EUV probe TG measurements, which can be performed on thick samples. We demonstrate the generation of SAWs at an acoustic wavelength in the sub-100 nm range in a bulk single crystal $SrTiO_3$ (STO) sample and present a methodology for measuring the SAW attenuation. STO, a prototypical perovskite material, was chosen for this study owing to the availability of single crystal samples with excellent surface quality as well as acoustic characterization data in the GHz range.[20–22] The experiment was conducted at the TIMER beamline at FERMI; a description of the apparatus is provided in Refs. 18 and 23. Figure 1 schematically shows the experimental arrangement. Pump pulses with the wavelength $\lambda_{ex} = 39.9$ nm and a probe pulse with the wavelength $\lambda_p = 13.3$ nm were derived from the FERMI FEL2 source and had a duration of ~70 fs. Two pump pulses were crossed at the sample surface at an angle of 27.6° to form an interference pattern with the period $\Lambda = 83.6$ nm. The time-delayed probe pulse was incident at an angle of 4.6°. The total pump energy at the sample was 0.6 μJ, the probe energy was 1.2 μJ; the spot size for pump and probe beams

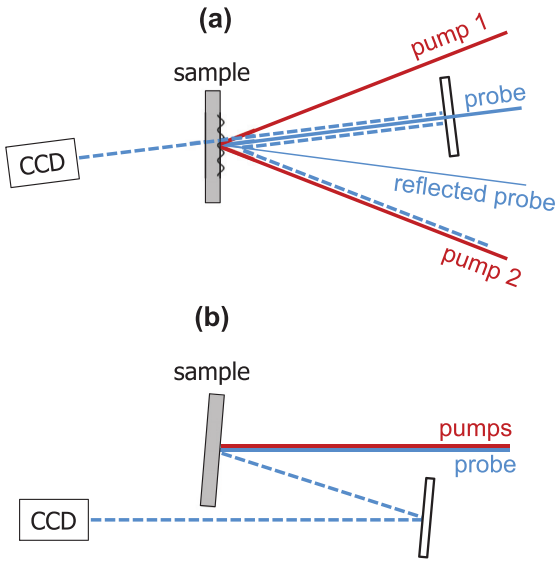

FIG. 1. Experimental arrangement: (a) top view and (b) side view. Sinusoidal surface displacement produced by the pump pulses acts as a transient diffraction grating for the probe beam; the ±1 diffraction orders are shown by dashed lines.

(defined as a diameter at the 1/e intensity level) was about 300 μm. The pump polarization was circular (chosen to facilitate the stable operation of the FEL but not essential for our experiment), while the probe polarization was vertical in terms of Fig. 1(b).

The sample was a (001) STO single crystal. The attenuation length of the 39.9 nm radiation in STO was 8 nm.[24] The absorption of the radiation led to a sinusoidal temperature profile along the sample surface (thermal grating) with the period Λ, and the resulting rapid thermal expansion launched counter-propagating SAWs at the same wavelength Λ.[5] The SAW wavevector direction determined by the orientation of the pump interference pattern on the sample was ⟨100⟩.[25] Both the thermal grating and SAWs modulated the surface profile, creating a transient reflective grating for the probe pulse. We used a multilayer mirror (reflectivity 69%) to pick up one of the diffraction orders, with the sample being tilted by 10° to separate the incident probe beam and the diffracted signal vertically, as shown in Fig. 1(b). The diffracted beam was reflected by the mirror, passed underneath the sample, and was detected by a CCD camera. The signal was averaged over 500 FEL shots per pump–probe delay point with the FEL repetition rate of 50 Hz.

For surface displacements much smaller than the probe wavelength, near-normal incidence, and $\Lambda \gg \lambda_p$, the diffraction efficiency of a reflecting diffraction grating with a sinusoidal surface displacement profile $u_z = u_0 \cos qx$, where $q = 2\pi/\Lambda$, is given by[26]

$$\eta = \frac{I_d}{I_p} = Rk_p^2 u_0^2, \tag{1}$$

where I_p and I_d are the intensities of the incident probe and diffracted beams, respectively, R is the reflection coefficient, k_p is the probe wave vector, and u_0 is the amplitude of the vertical surface displacement. The reflectivity of STO for near-normal incidence at 13.3 nm calculated based on Ref. 24 is quite small, $R = 6.2 \times 10^{-4}$. However, the poor reflectivity compared to visible wavelengths is offset by the large value of k_p. As a result, for an equal surface displacement amplitude, the diffraction efficiency at $\lambda_p = 13.3$ nm is about five times higher than at 500 nm, where $R = 0.18$ (of course in the latter case, the grating period would need to be much larger).

Figure 2 shows the diffracted signal as a function of the pump–probe delay. The slowly decaying component is due to the thermal grating, which decays via heat conduction, whereas the oscillations are due to the standing wave formed by counter-propagating SAWs. The experimentally measured diffraction efficiency at the signal maximum is 1.3×10^{-9}.[27] Using Eq. (1), we estimate the maximum amplitude of the surface displacement at 19 pm. This roughly agrees with an estimate of the surface displacement in the thermal grating based on the pump fluence, specific heat, and thermal expansion coefficient of STO,[28,29] which yields about 26 pm.[30]

The Fourier spectrum of the oscillations (with the slow background subtracted) shown in the inset in Fig. 2 reveals two frequencies, 51.7 and 103.4 GHz. The lower frequency yields a phase velocity of 4320 m/s, which agrees with the literature data for the SAW velocity in the [100] direction on the (001) plane of STO.[20] The presence of the "second harmonic" oscillations is due to the quadratic dependence of the signal on the surface displacement. The vertical surface displacement amplitude due to the thermal grating and counter-propagating SAWs is given by

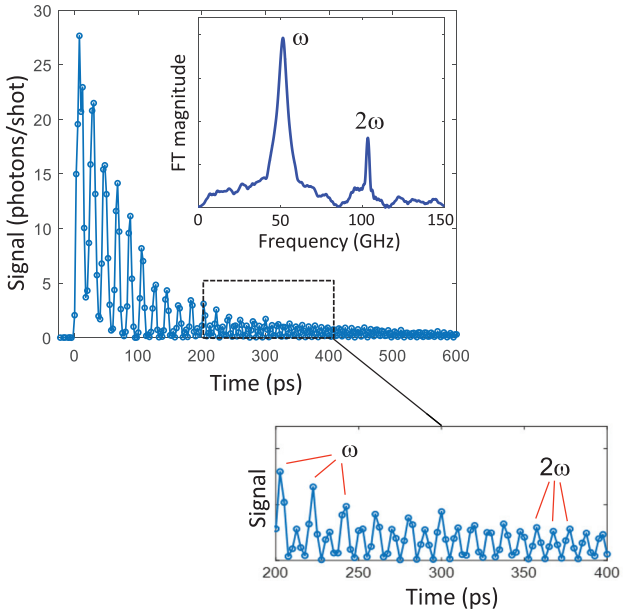

FIG. 2. Diffracted signal vs pump–probe delay time. The inset shows the Fourier spectrum of the oscillations. The bottom panel presenting the signal between 200 and 400 ps shows how oscillations at the SAW frequency ω decay and oscillations at 2ω become dominant at longer delays.

$$u_0 = S_{th}(t) + Ae^{-t/\tau}\cos\omega t, \tag{2}$$

where $S_{th}(t)$ describes the decaying amplitude of the thermal grating,[31] $A/2$ is the amplitude of each of the counter-propagating SAWs, τ is the SAW decay time, and ω is the SAW angular frequency given by $\omega = cq$, where c is the SAW velocity. Consequently, the time dependence of the diffraction signal is given by

$$\eta \propto S_{th}^2(t) + 2AS_{th}(t)e^{-t/\tau}\cos\omega t + \frac{1}{2}A^2e^{-2t/\tau}(1+\cos 2\omega t). \tag{3}$$

The frequency ω appears in the second term, which contains a product of the thermal and acoustic contributions. (One can think of this term as "heterodyne" detection of SAWs with the thermal grating providing a local oscillator.) Evidently, in our experiment, the thermal grating decay time is significantly shorter than the acoustic attenuation time τ: in this case, once the thermal grating decays, the first and second terms vanish and only the third term containing oscillations at 2ω remains. Indeed, as one can see in the bottom panel in Fig. 2, oscillations at 2ω become dominant in the tail of the signal. This is consistent with the fact that the 2ω peak in the spectrum is narrower than the ω peak: the width of the former is controlled by the SAW attenuation, while the width of the latter is dominated by the faster thermal decay.

According to Eq. (3), the oscillations at ω are not too useful for measuring the SAW decay time τ, as their decay is primarily controlled by the decay of the thermal grating. However, the decay time of the 2ω oscillations is independent of the thermal grating and given by $\tau/2$. Therefore, our strategy for measuring the SAW attenuation is to focus on the 2ω oscillations in the tail of the signal instead of analyzing the entire signal waveform. Fig. 3 shows the signal between 350 and 600 ps; toward the longest delays the signal maxima correspond to a

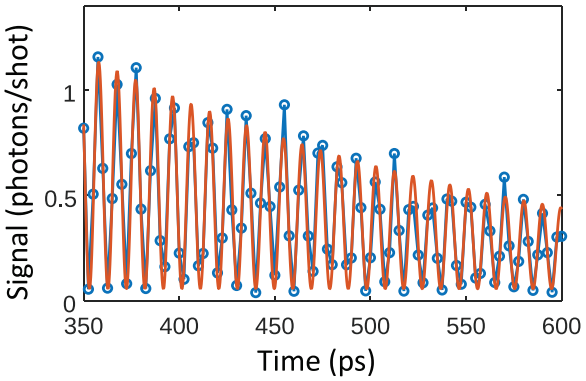

FIG. 3. The tail of the signal waveform (experimental data, blue) and the best fit with Eq. (4) (orange).

surface displacement amplitude of just ~2.5 pm. We fit this signal by the functional form

$$\eta = Be^{-2t/\tau}[1+\cos(2\omega t+\phi)] + C, \tag{4}$$

where a small offset C accounts for the background signal due to parasitically scattered light, which could not be entirely eliminated by the background subtraction performed during the data processing. The best fit yields $\tau = 472 \pm 20$ ps.[32] (The standard error was estimated from the behavior of χ^2 in the parameter space in the vicinity of the best fit, recognizing that this provides only a rough estimate of the experimental error;[33] within the constraints of the beamline experiment, we could not perform multiple pump–probe delay scans for a proper statistical analysis.) The normally reported "phonon lifetime" corresponds to $1/e$ decay for the acoustic intensity rather than amplitude and is equal to $\tau/2$. The $1/e$ intensity attenuation length, or the surface phonon mean free path, is equal to 1.0 μm.

Previously, the acoustic attenuation in STO at comparable frequencies was only measured for bulk longitudinal waves. The SAW consists of longitudinal and transverse inhomogeneous waves;[34] therefore, it would be, in principle, possible to combine the SAW and bulk longitudinal data to obtain the attenuation of transverse waves. However, the reported values of τ at 300 K for longitudinal waves in STO vary within a wide range 400–1400 ps.[21,22] Also, the observed SAW attenuation, besides the intrinsic attenuation due to lattice anharmonicity,[35] may include extrinsic attenuation due to surface roughness;[36] hence, the measured surface phonon lifetime should be considered a lower bound for the intrinsic lifetime. Elucidating the relative roles of the extrinsic and intrinsic contributions requires a further study and goes beyond the scope of the present report. Yet another potential contributor to the observed attenuation is the "walk-off" effect[37] owing to the finite spatial width of the counter-propagating SAW wavepackets: when the wavepackets no longer overlap, there is no standing wave and the oscillations in the signal vanish. The wavepacket width is determined by the extent of the high-contrast interference pattern, which was ~70 μm at the pump crossing angle we used.[38] Since this width was much greater than the SAW attenuation length, the walk-off effect was negligible.

In conclusion, the described approach provides a way to generate ultrahigh frequency SAWs in a broad range of materials without

nanofabrication. Unlike the conventional laser excitation of SAWs, this technique is not limited to optically opaque materials, since all materials are highly absorbing in the EUV range. The current setup at FERMI already makes it possible to conduct transient grating measurements at grating periods as short as 28 nm,[18] and with shorter excitation wavelengths, a further extension of the wavelength range down to ∼10 nm is possible. This will push the SAW frequency close to 1 THz and close the gap in surface phonon spectroscopy between surface Brillouin scattering operating in the wavelength range above ∼300 nm (Refs. 20 and 39) and He atom scattering, whose limited energy resolution restricts the useful surface phonon wavelength to below ∼10 nm.[40] Furthermore, TG spectroscopy, as a time-domain technique, is not limited by the spectrometer resolution, which is especially useful for measuring the SAW attenuation. (In this regard, the only practical limitation is the length of the probe delay line.) For example, to measure the SAW decay time obtained in this work, one would need a spectrometer resolution of ∼0.01 meV, while the resolution of He atom scattering spectroscopy is typically 0.5–1 meV.[40]

SAW attenuation measurements will be useful for the development of SAW devices: currently, the propagation loss can only be assessed indirectly via the Q factor of the device.[41,42] While SAW devices with frequencies up to 30 GHz are being developed,[43] there are no data on SAW attenuation above ∼10 GHz in any material, and even measurements at lower frequencies are difficult and rarely done: for example, Ref. 12 reported measurements of SAW attenuation in Si at 7 GHz performed using laser excitation and detection mediated by nanostructures, which required the fabrication of a series of "excitation" and "detection" nanostructures separated by a variable distance. The EUV TG technique described here enables direct measurements of the SAW attenuation without any nanofabrication and at much higher frequencies than any of the existing methods allows. Furthermore, precise measurements of the high-wavevector SAW dispersion will help in the characterization of ultrathin films[11] and, more generally, near-surface mechanical properties of materials. While the current experiment required an FEL facility, further progress in the high harmonic generation[10,11] is likely to enable EUV TG spectroscopy with a table-top setup. Finally, we expect that the reflection-mode EUV TG arrangement will be useful for studying a broad range of phenomena beyond surface acoustic waves, including thermal transport,[7] nonlinear optics,[44] and ultrafast nanoscale magnetism.[38]

The contribution of A.A.M., R.A.D., and K.A.N. was supported by the U.S. Department of Energy, Office of Basic Energy Sciences, under Award No. DE-SC0019126. V.U. and S.B. acknowledge support from the European Research Council, Starting Grant No. 715452 MAGNETIC-SPEED-LIMIT. G.C. and Z.D. acknowledge support in part by the Office of Naval Research under MURI Grant No. N00014-16-1-2436 via UT Austin.

DATA AVAILABILITY

The data that support the findings of this study are available from the corresponding author upon reasonable request.

REFERENCES

[1]R. E. Lee and R. M. White, Appl. Phys. Lett. **12**, 12 (1968).
[2]A. A. Maznev, A. A. Kolomenskii, and P. Hess, Phys. Rev. Lett. **75**, 3332 (1995).
[3]A. M. Lomonosov, P. Hess, and A. P. Mayer, Phys. Rev. Lett. **88**, 076104 (2002).
[4]N. Boechler, J. K. Eliason, A. Kumar, A. A. Maznev, K. A. Nelson, and N. Fang, Phys. Rev. Lett. **111**, 036103 (2013).
[5]J. A. Rogers, A. A. Maznev, M. J. Banet, and K. A. Nelson, Annu. Rev. Mater. Sci. **30**, 117 (2000).
[6]A. Lomonosov, A. P. Mayer, and P. Hess, in *Modern Acoustical Techniques for the Measurement of Mechanical Properties*, edited by M. Levy, H. E. Bass, and R. Stern (Academic, Boston, 2001), Vol. 39, pp. 65–134.
[7]F. Hofmann, M. P. Short, and C. A. Dennett, MRS Bull. **44**, 392 (2019).
[8]An optical intensity pattern formed by far-field focusing/imaging cannot contain Fourier components with a period smaller than half wavelength; consequently, SAWs with a smaller wavelength cannot be excited unless a strongly nonlinear mechanism such as ablation is employed. Likewise. SAWs with a wavelength smaller than half the optical wavelength will be "invisible" to the optical probe beam.
[9]D. H. Hurley and K. L. Telschow, Phys. Rev. B **66**, 153301 (2002).
[10]M. E. Siemens, Q. Li, M. M. Murnane, H. C. Kapteyn, R. Yang, E. H. Anderson, and K. A. Nelson, Appl. Phys. Lett. **94**, 093103 (2009).
[11]J. N. Hernandez-Charpak, K. M. Hoogeboom-Pot, Q. Li, T. D. Frazer, J. L. Knobloch, M. Tripp, S. W. King, E. H. Anderson, W. Chao, M. M. Murnane, H. C. Kapteyn, and D. Nardi, Nano Lett. **17**, 2178 (2017).
[12]D. Li and D. G. Cahill, Phys. Rev. B **94**, 104306 (2016).
[13]D. Attwood and A. Sakdinawat, *X-Rays and Extreme Ultraviolet Radiation: Principles and Applications* (Cambridge University Press, Cambridge, 2016).
[14]A. A. Maznev, F. Bencivenga, A. Cannizzo, F. Capotondi, R. Cucini, R. A. Duncan, T. Feurer, T. D. Frazer, L. Foglia, H.-M. Frey, H. Kapteyn, J. Knobloch, G. Knopp, C. Masciovecchio, R. Mincigrucci, G. Monaco, M. Murnane, I. Nikolov, E. Pedersoli, A. Simoncig, A. Vega-Flick, and K. A. Nelson, Appl. Phys. Lett. **113**, 221905 (2018).
[15]E. Allaria, D. Castronovo, P. Cinquegrana, P. Craievich, M. Dal Forno, M. B. Danailov, G. D'Auria, A. Demidovich, G. De Ninno, S. D. Mitri, B. Diviacco, W. M. Fawley, M. Ferianis, E. Ferrari, L. Froehlich, G. Gaio, D. Gauthier, L. Giannessi, R. Ivanov, B. Mahieu, N. Mahne, I. Nikolov, F. Parmigiani, G. Penco, L. Raimondi, C. Scafuri, C. Serpico, P. Sigalotti, S. Spampinati, C. Spezzani, M. Svandrlik, C. Svetina, M. Trovo, M. Veronese, D. Zangrando, and M. Zangrando, Nat. Photon. **7**, 913 (2013).
[16]H. J. Eichler, P. Günter, and D. Pohl, *Laser-Induced Dynamic Gratings* (Springer-Verlag, Berlin, 1986).
[17]F. Bencivenga, R. Cucini, F. Capotondi, A. Battistoni, R. Mincigrucci, E. Giangrisostomi, A. Gessini, M. Manfredda, I. P. Nikolov, E. Pedersoli, E. Principi, C. Svetina, P. Parisse, F. Casolari, M. B. Danailov, M. Kiskinova, and C. Masciovecchio, Nature **520**, 205 (2015).
[18]F. Bencivenga, R. Mincigrucci, F. Capotondi, L. Foglia, D. Naumenko, A. A. Maznev, E. Pedersoli, A. Simoncig, F. Caporaletti, V. Chiloyan, R. Cucini, F. Dallari, R. A. Duncan, T. D. Frazer, G. Gaio, A. Gessini, L. Giannessi, S. Huberman, H. Kapteyn, J. Knobloch, G. Kurdi, N. Mahne, M. Manfredda, A. Martinelli, M. Murnane, E. Principi, L. Raimondi, S. Spampinati, C. Spezzani, M. Trovò, M. Zangrando, G. Chen, G. Monaco, K. A. Nelson, and C. Masciovecchio, Sci. Adv. **5**, eaaw5805 (2019).
[19]D. Naumenko, R. Mincigrucci, M. Altissimo, L. Foglia, A. Gessini, G. Kurdi, I. Nikolov, E. Pedersoli, E. Principi, A. Simoncig, M. Kiskinova, C. Masciovecchio, F. Capotondi, and F. Bencivenga, ACS Appl. Nano Mater. **2**, 5132 (2019).
[20]J. D. Huang, M. H. Kuok, H. S. Lim, and S. C. Ng, J. Appl. Phys. **94**, 7341 (2003).
[21]C.-Y. Yang and K.-H. Lin, Phys. Rev. B **98**, 064308 (2018).
[22]L. Maerten, A. Bojahr, M. Reinhardt, A. Koreeda, M. Rössle, and M. Bargheer, arXiv:1810.00381 (2018).
[23]R. Mincigrucci, L. Foglia, D. Naumenko, E. Pedersoli, A. Simoncig, R. Cucini, A. Gessini, M. Kiskinova, G. Kurdi, N. Mahne, M. Manfredda, I. P. Nikolov, E. Principi, L. Raimondi, M. Zangrando, C. Masciovecchio, F. Capotondi, and F. Bencivenga, Nucl. Instrum. Methods Phys. Res., Sect. A **907**, 132 (2018).
[24]B. L. Henke, E. M. Gullikson, and J. C. Davis, At. Data Nucl. Data Tables **54**, 181 (1993).
[25]The SAW wavevector direction can be easily varied by rotating the sample. While for some directions a pseudo-SAW mode can be excited in addition to

the true SAW,[34] there is no such complication for the ⟨100⟩ direction on the (001) surface.
[26]J. E. Harvey and R. N. Pfisterer, Opt. Eng. **59**, 017103 (2020).
[27]The calculation of the diffraction efficiency accounted for the reflectance of the multilayer mirror, transmission of the Zr filter in front of the CCD camera (0.46) and the quantum efficiency of the camera (0.85).
[28]A. Durán, F. Morales, L. Fuentes, and J. M. Siqueiros, J. Phys.: Condens. Matter **20**, 085219 (2008).
[29]K. Munakata and A. Okazaki, Acta Crystallogr., Sect. A **60**, 33 (2004).
[30]We caution the reader that both numbers are underestimates. The calculated displacement does not include the SAW contribution and does not account for Poisson's ratio, which makes the displacement amplitude larger.[31] The measured diffraction efficiency is also an underestimate, since the high contrast interference pattern only occupies about 1/4 of the pump/probe spot.[38]
[31]O. W. Käding, H. Skurk, A. A. Maznev, and E. Matthias, Appl. Phys. A **61**, 253 (1995).
[32]The best fit values of other parameters: $\omega/2\pi = 51.7$ GHz, $\phi = 0.061$, and $C = 0.055$ photons/shot.
[33]W. H. Press, S. A. Teukolsky, W. T. Vetterling, and B. P. Flannery, *Numerical Recipes: The Art of Scientific Computing* (Cambridge University Press, New York, 2007).
[34]G. W. Farnell, in *Physical Acoustics*, edited by W. I. Mason and R. N. Thurston (Academic Press, New York, 1970), Vol. 6, p. 109.
[35]H. J. Maris, in *Physical Acoustics*, edited by W. P. Mason and R. N. Thurston (Academic, New York, 1971), Vol. 8, p. 279.
[36]A. A. Maradudin and D. L. Mills, Ann. Phys. **100**, 262 (1976).
[37]Y.-X. Yan and K. A. Nelson, J. Chem. Phys. **87**, 6240 (1987).
[38]D. Ksenzov, A. A. Maznev, V. Unikandanunni, F. Bencivenga, F. Capotondi, A. Caretta, L. Foglia, M. Malvestuto, C. Masciovecchio, R. Mincigrucci, K. A. Nelson, M. Pancaldi, E. Pedersoli, L. Randolph, H. Rahmann, S. Urazhdin, S. Bonetti, and C. Gutt, Nano Lett. **21**, 2905 (2021).
[39]P. Mutti, C. E. Bottani, G. Ghislotti, M. Beghi, G. A. D. Briggs, and J. R. Sandercock, in *Advances in Acoustic Microscopy*, edited by G. A. D. Briggs (Springer, New York, 1995), Vol. 1, pp. 249–300.
[40]J. P. Toennies, in *Surface Phonons*, edited by W. Kress and F. W. de Wette (Springer, Berlin/Heidelberg, 1991), pp. 111–166.
[41]S. Fujii, T. Odawara, H. Yamada, T. Omori, K. Hashimoto, H. Torii, H. Umezawa, and S. Shikata, IEEE Trans. Ultrason. Ferroelectr. Freq. Control **60**, 986 (2013).
[42]V. J. Gokhale, B. P. Downey, M. T. Hardy, E. N. Jin, J. A. Roussos, and D. J. Meyer, in *IEEE 33rd International Conference on Micro Electro Mechanical Systems (MEMS)* (IEEE, Vancouver, BC, Canada, 2020), pp. 1262–1265.
[43]J. Zheng, J. Zhou, P. Zeng, Y. Liu, Y. Shen, W. Yao, Z. Chen, J. Wu, S. Xiong, Y. Chen, X. Shi, J. Liu, Y. Fu, and H. Duan, Appl. Phys. Lett. **116**, 123502 (2020).
[44]R. Bohinc, G. Pamfilidis, J. Rehault, P. Radi, C. Milne, J. Szlachetko, F. Bencivenga, F. Capotondi, R. Cucini, L. Foglia, C. Masciovecchio, R. Mincigrucci, E. Pedersoli, A. Simoncig, N. Mahne, A. Cannizzo, H. M. Frey, Z. Ollmann, T. Feurer, A. A. Maznev, K. Nelson, and G. Knopp, Appl. Phys. Lett. **114**, 181101 (2019).